Brazilian Journal
of Chemical
Engineering

ISSN 0104-6632
Printed in Brazil
www.abeq.org.br/bjche

Vol. 24, No. 04, pp. 587 - 595, October - December, 2007

CFD PREDICTIONS OF DRILLING FLUID VELOCITY AND PRESSURE PROFILES IN LAMINAR HELICAL FLOW

F. A. R. Pereira, M. A. S. Barrozo and C. H. Ataíde*

School of Chemical Engineering, Federal University of Uberlândia,
Phone: +(55)(34) 3239-4292, Building K, Campus Santa Mônica
P.O. 593, 38400-902, Uberlândia - MG, Brazil.
E-mail: chataide@ufu.br

(Received: March 29, 2005 ; Accepted: September 18, 2007)

Abstract - Fluid flow in annular spaces has received a lot of attention from oil industries, both in drilling operations and in petroleum artificial rising. In this work, through numerical simulation using the computational fluid dynamics (CFD) technique, the flow of non-Newtonian fluids through the annuli formed by two tubes in concentric and eccentric arrangements of a horizontal system has been investigated. The study analyzes the effects of viscosity, eccentricity, flow and shaft rotation on the tangential and axial velocity profiles and on the hydrodynamic losses. It evaluates the performance of the numerical method used, comparing the results obtained with those in other reported works, aiming to validate the simulation strategy by the interpolation routines as well as the couplings algorithms adopted.
Keywords: Annular flow; Drilling; Computational fluid dynamic (CFD).

INTRODUCTION

Since the beginning of the 80's, the petroleum industry has given prominence to fluid flow in annular spaces, both in oilwell drilling operations with cuttings transport by the drilling muds and also in oil artificial lifting by progressive cavity pump systems. Due to the constant concern with operational costs and the need for raising production capacity; higher flow rates have most frequently been used, and consequently, the hydrodynamic losses in the annular space between the wellbore and drillpipe began to require a significant amount of energy. So, this energy quantification has assumed a relevant role in dimensioning these units.

Cuttings are removed by pumping the drilling fluid from the surface into the wellbore through the inside of drillpipe, the drillbit lubricating, cooling and cleaning the cut region and avoiding unnecessary increases in torque requirements because of the accumulation of particles (Nouri et al., 1997). The drag of these particles is strongly related to the drilling mudflow velocity profiles in the annular space (Escudier et al., 2000), therefore, knowledge of "mud hydraulics" is directly associated with an efficient drilling operation.

Drilling muds are generally suspensions with rheological non-Newtonian behavior, some of the pseudoplastic and others of the viscoplastic type (with residual tension). Viscoplastic suspensions are used for situations where minimization of cuttings sedimentation is desired, in the case of interruption of fluid circulation (Sharma and Mahto, 2004).

The work available in the literature shows some idealizations, such as isothermal systems, well-defined rheology (different from the tixotropy found in real situations) and constant annular geometry, among others. Even though the problem of physical description is based on some assumptions, the phenomenon is highly complex, requiring the "mud

*To whom correspondence should be addressed

dynamicists" to use new tools for drilling fluid flowfield prediction, as proposed in Nouar et al. (1998) and Sharif and Hussain (2000).

Computational Fluid Dynamics

The physical aspects of any fluid flow are ruled by three main principles: the conservation of mass, the second law of Newton and the conservation of energy. These basic principles may be expressed in terms of mathematical equations, which are mostly partial differential equations. The computational fluid dynamics technique tries to solve the equations that rule the fluids flow numerically, while the mathematical solution advances in space and time to obtain the complete numerical flowfield description.

The comparison of the results of numerical fluid dynamics with experimental data has taken on an important role in validating and establishing limits of many approaches for the ruling equations. Traditionally, it has been shown to be an effective, low-cost alternative for total scale measures. This situation has lead to an increase in the development of numerical simulation routines and commercial codes.

The CFD technique emerged as a result of the current increase in computer processing speed and available memory. Currently, this branch of fluid dynamics complements experimental and theoretical work, providing economically interesting alternatives through the simulation of real flows and allowing an alternative form for theoretical advances under conditions unavailable experimentally.

The Finite Volumes Technique

Most of the numerical methods such as finite differences, finite elements and finite volumes, among others, are derived from the method of weighed residues. The minimization of residues in the finite volumes method is equivalent to the conservation principle for each control volume. When there is no overlapping of control volumes in a given neighborhood, it is possible to create a group of discrete equations that satisfy the overall conservation balance. The guarantee that the conservation principles will be satisfied at the global and elementary level makes the finite volumes method attractive and physically consistent.

In the finite volumes method, the type of coupling and interpolation functions to be used may be considered one of the main characteristics of a numerical model, responsible for the quality of the solution obtained.

NUMERICAL SIMULATION SETUP

Annular Geometry and Computational Mesh

In this study, the computational mesh represents a virtual flow system, formed by the configurations of two tubes (100 mm outer and 50 mm inner radius, both 6.0 m long). The annular geometry, formed by the space between the two tubes, has been configured in two arrangements, one with concentric tubes and the other one with an inner tube displacement, providing an eccentric layout. In this work, the eccentricity used was 0.80. In Figure 1 a longitudinal view of the ring arrangement for the concentric and the eccentric cases as well as the cell distribution in the computer grid is shown.

The three-dimensional meshes were assembled with Gambit®, a commercial code, using only hexahedric cells that provides the system with a structured mesh. In the eccentric geometry case, to achieve a distribution close to the normal (90º in relation to the inner cylinder), a strategy of dividing the cell into four quadrants with the centerline as the reference system was established. The cell distribution applied in each quadrant followed the "number of interval divisions" method, instead of the "fixed dimension division" distribution method, allowing a better fit in the annular region.

The concentric mesh layout has a total of 57,000 cells, while in the eccentric case the mesh has 68,400 cells. The latter has a larger number of cells due to a greater refinement of the region with a smaller annular space.

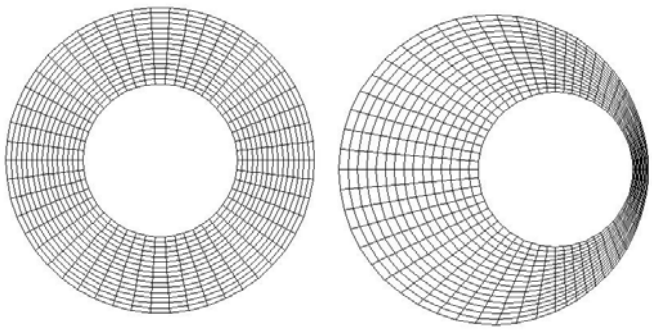

Figure 1: Cell distribution in the concentric and eccentric rings.

Flow Modeling

Assuming an isothermal, laminar, permanent and uncompressible flow of a fluid with effective viscosity depending only on the deformation tensor rate, the flow modeling may be described using the classical equations of continuity (equation 1) and the axial, radial and tangential components (equations 2, 3 and 4) of the momentum equation.

$$\frac{1}{r}\frac{\partial}{\partial r}\left(rv_r\right)+\frac{1}{r}\frac{\partial}{\partial \phi}\left(v_\phi\right)+\frac{\partial}{\partial z}\left(v_z\right)=0 \tag{1}$$

$$\rho\left(v_r\frac{\partial v_z}{\partial r}+\frac{v_\phi}{r}\frac{\partial v_z}{\partial \phi}+v_z\frac{\partial v_z}{\partial z}\right)= -\frac{\partial P}{\partial z}-\left(\frac{1}{r}\frac{\partial}{\partial r}\left(r\tau_{rz}\right)+\frac{1}{r}\frac{\partial \tau_{\phi z}}{\partial \phi}+\frac{\partial \tau_{zz}}{\partial z}\right)+\rho g_z \tag{2}$$

$$\rho\left(v_r\frac{\partial v_r}{\partial r}+\frac{v_\phi}{r}\frac{\partial v_r}{\partial \phi}-\frac{v_\phi^2}{r}+v_z\frac{\partial v_\phi}{\partial z}\right)= -\frac{\partial P}{\partial r}-\left(\frac{1}{r}\frac{\partial}{\partial r}\left(r\tau_{rr}\right)+\frac{1}{r}\frac{\partial \tau_{r\phi}}{\partial \phi}-\frac{\tau_{\phi\phi}}{r}+\frac{\partial \tau_{rz}}{\partial z}\right)+\rho g_r \tag{3}$$

$$\rho\left(v_r\frac{\partial v_\phi}{\partial r}+\frac{v_\phi}{r}\frac{\partial v_\phi}{\partial \phi}+\frac{v_r v_\phi}{r}+v_z\frac{\partial v_\phi}{\partial z}\right)= \frac{1}{r}\frac{\partial P}{\partial \phi}-\left(\frac{1}{r^2}\frac{\partial}{\partial r}\left(r^2\tau_{r\phi}\right)+\frac{1}{r}\frac{\partial \tau_{\phi\phi}}{\partial \phi}+\frac{\partial \tau_{\phi z}}{\partial z}\right)+\rho g_\phi \tag{4}$$

Non-Newtonian flows have the shear tension in terms of effective viscosity and deformation tensor rate (equation 5). Effective viscosity is a function of the three invariants of deformation tensor rate. In the numerical simulations developed in this study, the classical hypothesis that considers only the effect of the second invariant was adopted (equations 6 and 7).

$$\bar{\tau}=\mu\left(\bar{\gamma}\right)\bar{\gamma} \tag{5}$$

$$\dot{\gamma}=\sqrt{\bar{\gamma}:\bar{\gamma}} \tag{6}$$

$$\dot{\gamma}^2=2\left[\left(\frac{\partial v_r}{\partial r}\right)^2+\left(\frac{1}{r}\frac{\partial v_\phi}{\partial \phi}+\frac{v_r}{r}\right)^2+\left(\frac{\partial v_z}{\partial z}\right)^2\right]+ \left[r\frac{\partial}{\partial r}\left(\frac{v_\phi}{r}\right)+\frac{1}{r}\frac{\partial v_r}{\partial \phi}\right]^2+\left[\frac{1}{r}\frac{\partial v_z}{\partial \phi}+\frac{\partial v_\phi}{\partial z}\right]^2+ \left[\frac{\partial v_r}{\partial z}+\frac{\partial v_z}{\partial r}\right]^2 \tag{7}$$

Fluids Characterization

The fluids used in the numerical simulations in this work are non-Newtonian and time-independent with a viscoplastic behavior, where viscosity decreases with an increase in deformation rate. The model with three parameters of Cross (1965) was chosen to represent the rheological behavior of two fluids (equation 8). The parameter values used in the simulations, estimated from the results obtained by Escudier et al. (2002), can be found in Table 1.

$$\mu_{ef}=\frac{\mu_0}{1+\left(\lambda\dot{\gamma}\right)^{1-n}} \tag{8}$$

Table 1: Rheologic parameters, based on the model of Cross (1965).

Cross parameters	Fluid 1	Fluid 2
μ_0 (kg/ms)	0.1775	0.1834
λ (s)	2.5684	0.4737
n (–)	0.5485	0.4852

Dimensionless Parameters

For a better comprehension of the flow conditions studied, some information based on dimensionless parameters will be reported, favoring comparison with some results reported in the literature. Some of the dimensionless parameters presented follow classical concepts, making a demonstration unnecessary.

Eccentricity (e): indicates the level of radial displacement from the inner radius (R_{int}) in relation to the outer radius (R_{ext}).

$$e=\frac{\text{distance between centers}}{R_{ext}-R_{int}} \tag{9}$$

Axial dimensionless velocity (U_a): ratio between the local axial velocity (v_z) and the inlet velocity (v_{inlet}).

$$U_a = \frac{v_z}{v_{inlet}} \tag{10}$$

Tangential dimensionless velocity (V_a): ratio between the local tangential velocity (v_ϕ) and the angular velocity (w) times the inner axis radius (R_{int})

$$V_a = \frac{v_\phi}{wR_{int}} \tag{11}$$

Reynolds number (Re_G): classical parameter for the description of flow states, in this case, generalized Reynolds, for non-Newtonian fluid with effective viscosity (μ_{ef}).

$$Re_G = \frac{2\rho U_a \left(R_{ext} - R_{int}\right)}{\mu_{ef}} \tag{12}$$

Dimensionless annular space (G_a): indicated by the radial position in relation to the annular space.

$$G_a = \frac{\text{radial distance between the outer wall and inner axis}}{\text{annular space}} \tag{13}$$

Numerical Simulation

In order to calculate the velocity components, the ruling equations were integrated in each computational mesh cell throughout the domain, being discretized following the finite volumes approach. Then they were linearized and solved numerically. The calculations were done using the pressure discretization scheme following the PRESTO routine. For the pressure-velocity coupling the SIMPLEC algorithm was applied and for the momentum interpolation, the QUICK routine was chosen due to its better adaptation to hexahedric meshes. The commercial code used to simulate the strategy described was Fluent® version 6.2.16.

The coordinate reference system was fixed on the inner tube origin axis for both situations: the concentric and the eccentric.

Aiming to validate the numerical method employed in this work, a set of simulations was carried out based on the work published by Escudier et al. (2002), where the authors experimentally determined the axial and tangential velocity profiles using laser anemometry (Doppler laser). Based on these experimental data, the authors also presented a comparative study of numerical simulation in a two-dimensional system. In the Escudier et al. (2002) work, although the information about the velocity profile is very detailed, not much about the pressure losses affected by their main variables is discussed. In Table 2 two conditions experimentally studied by Escudier et al. (2002) that have been simulated in this work are shown.

Intending to explore the effects of flow rate, inner cylinder rotation and fluid rheology on pressure loss, 34 other conditions were numerically simulated. In Table 3 the conditions implemented are shown.

For the eccentricity case with an inlet velocity of 0.203 m/s and an inner shaft rotation, the results were not considered, since the values from these simulations showed “reverse flow”. This occurred due to the combination of three factors: high viscosity associated with a reduced inlet velocity and high inner axis rotation. This reverse flow condition was numerically unstable as determined by analysis of the residues, mainly with the continuity equation.

Table 2: Simulation conditions for validation.

Eccentricity	v (m/s)	w (rad/s)	Fluid
0.0	0.203	5.24	Fluid 1
0.8	0.268	5.35	Fluid 2

Table 3: Conditions used in the simulation.

e (-)	v (m/s)	w (rad/s)	Fluids	Re_G (-)
0.00	0.203 0.406 0.609	0.0; 2.56 and 5.24 0.0; 2.56 and 5.24 0.0; 2.56 and 5.24	Fluids 1 and 2	355 to 1598
0.80	0.203 0.406 0.609	0.0 0.0; 2.56 and 5.24 0.0; 2.56 and 5.24	Fluids 1 and 2	218 to 934

RESULTS AND DISCUSSION

The results obtained will be presented in two parts: the first has the purpose of indetifying the validation conditions of the numerical method applied, mainly in regards to the pressure-velocity coupling algorithm and considering the experimental results from Escudier et al. (2002). In the second part a set of numerical simulations developed to obtain more information about the main variables that affect the pressure drop in the horizontal annular flow are presented.

Determination of the Velocity Profiles

Focusing on the two tube configurations, concentric and eccentric, the non-Newtonian laminar helical flow was evaluated in the situations described previously. Typical results shows the effect of eccentricity on the axial dimensionless velocity contours of a fully developed flow without shaft rotation, which may be seen in Figures 2 and 3.

The qualitative effect of the inner cylinder rotation is shown in Figure 4, in terms of the axial dimensionless velocity for a shaft angular velocity of 5.35 rad/s.

The results shown in Figures 3 and 4 reflect flow situations similar to information on the effect of shaft rotation found in the literature. In the eccentric geometry with a narrow annular space, for example, the same stagnation regions as the ones reported by Martins et al. (1999) were observed. The results shown in Figure 4 shows not only the rotation effect on the reduction of stagnation regions, but also the direction of core flow displacement in the lower region of the tube. These effects are relevant in cleaning operations and cuttings transportation in horizontal drilling systems.

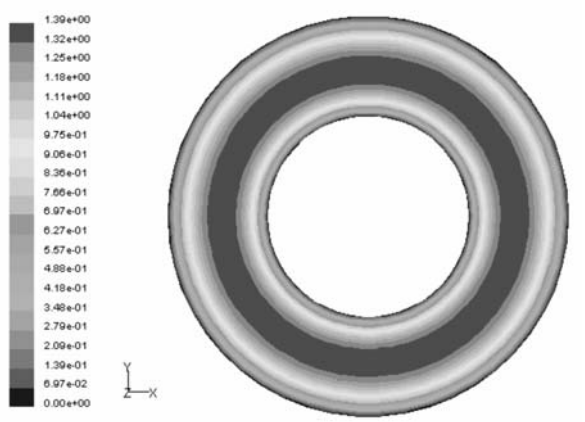

Figure 2: Dimensionless axial velocity in the concentric layout without shaft rotation.

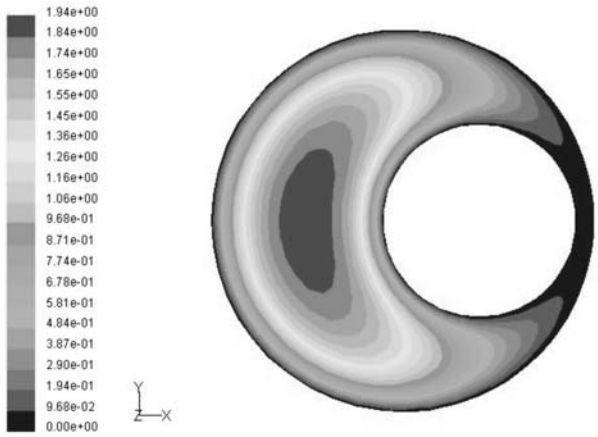

Figure 3: Dimensionless axial velocity in the eccentric layout without shaft rotation.

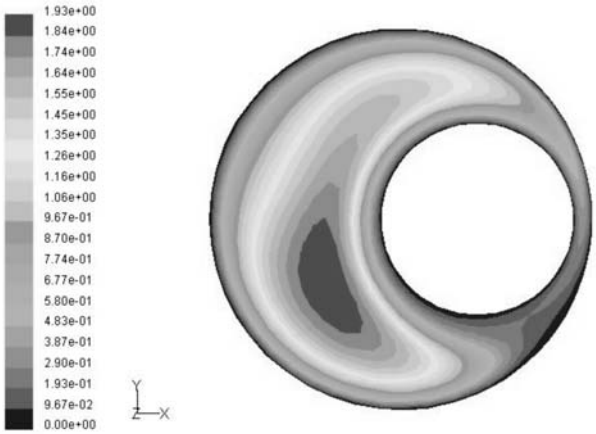

Figure 4: Dimensionless axial velocity in the eccentric layout with 5.35 rad/s.

The velocity profile results for helical flow are usually presented using Cartesian charts, where the x-axis of the system is the reference. Figures 5, 6 and 7 contain a comparison of the simulation results obtained in this work with the experimental data of Escudier et al. (2002), for concentric and eccentric cases (Table 2). The axial (U_a) and tangential (V_a) dimensionless profiles are plotted as a function of dimensionless annular space (G_a). As a function of its symmetry plan, the concentric case has the same annular space between the tubes for any position; although, in the eccentric case, there are two annular spaces represented in the figures, defined as $(G)_{large}$ and $(G)_{slim}$.

The agreement between the results presented in Figures 5, 6 and 7 allowed validation of the numerical method, particularly the algorithm for velocity and pressure coupling, applied in these simulations.

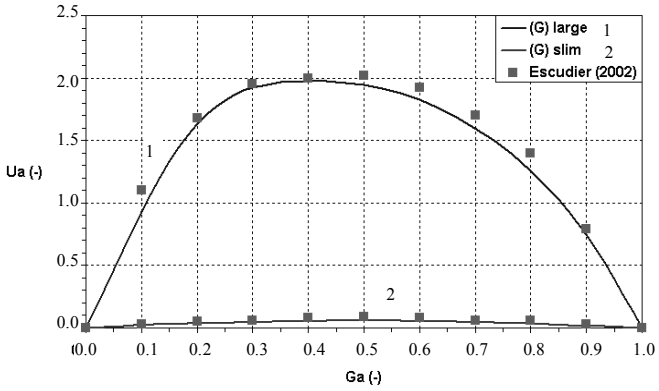

Figure 5: Dimensionless profiles of axial and tangential velocities for e=0.00.

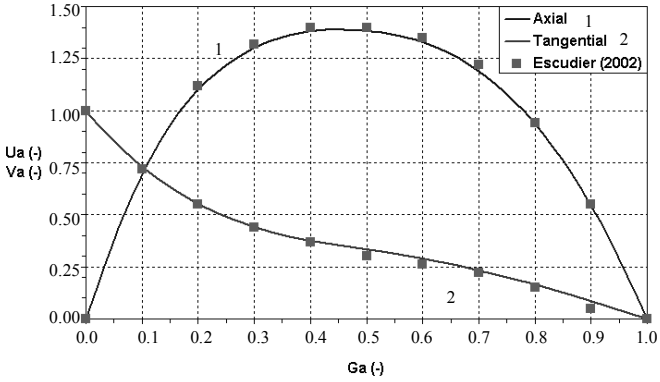

Figure 6: Dimensionless profiles of axial velocities for e=0.80.

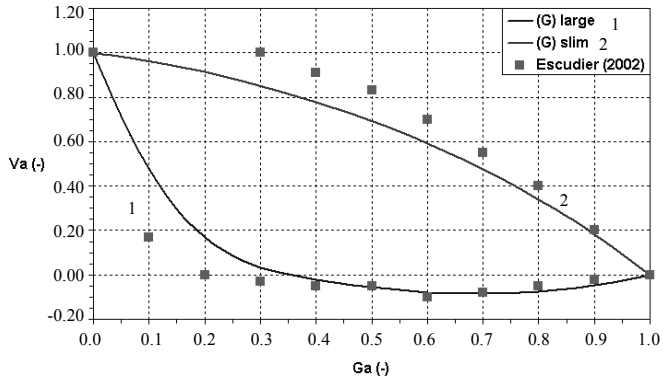

Figure 7: Dimensionless profiles of tangential velocities for e=0.80.

The Effect of Operational Variables on Pressure Drop

The pressure drop was determined along the system axial direction. For Fluid 1, the effect of flow rate and inner cylinder rotation on the pressure drop are presented in Figures 8 and 9, for the concentric and eccentric cases respectively.

In the same way, for Fluid 2, the effect of flow rate and inner cylinder rotation on the system pressure drop are presented in Figures 10 and 11, for the concentric and eccentric cases respectively.

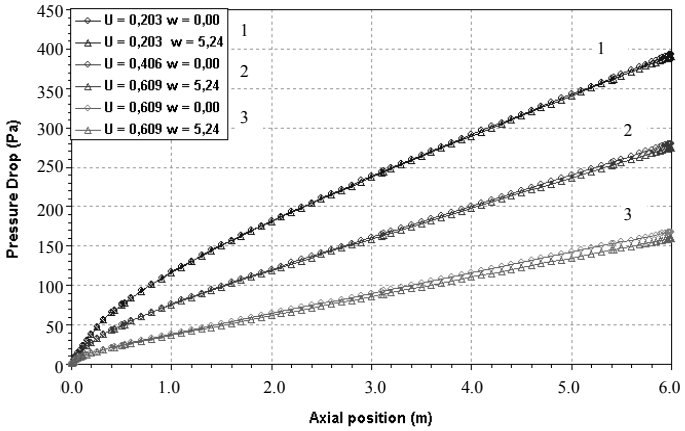

Figure 8: Effect of flow rate and shaft rotation on pressure drop.

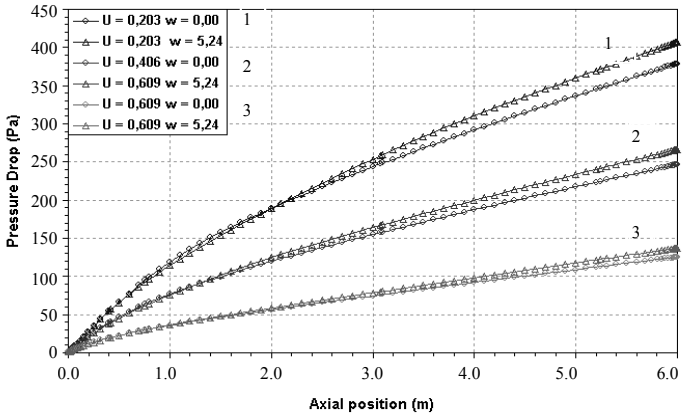

Figure 9: Effect of flow rate, shaft rotation and eccentricity on pressure drop.

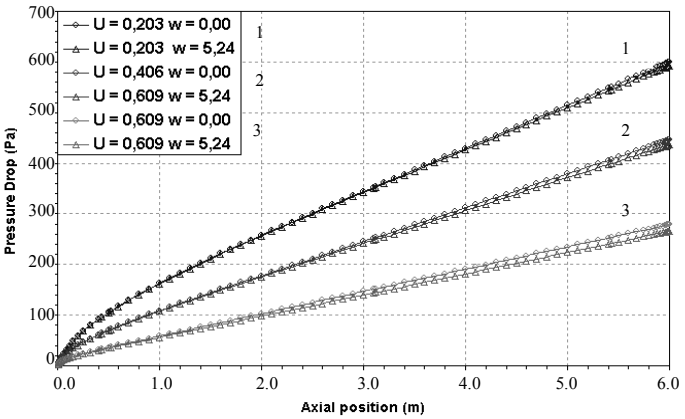

Figure 10: Effect of flow rate and shaft rotation on pressure drop.

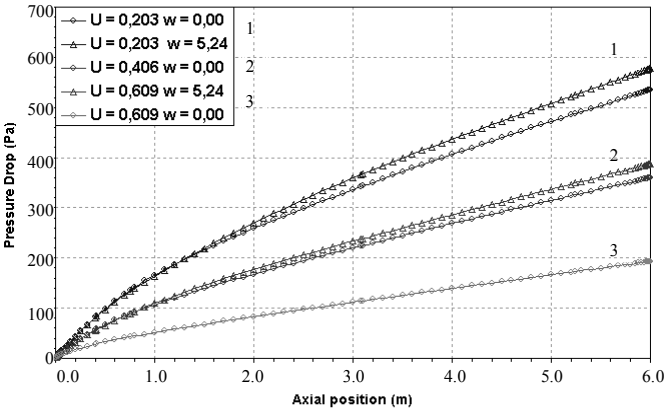

Figure 11: Effect of flow rate, shaft rotation and eccentricity on pressure drop.

Analyzing Figures 8, 9, 10 and 11, the following aspects can be stressed:

- As expected, the fluids flow rate was the operational variable with the highest impact on the pressure drop.
- The values of pressure drop for cases with a rotation of 2.56 rad/s were in between the values for cases with no rotation and with a rotation of 5.24 rad/s. In order to help visualize the results and interpret the graphics, the graphic presentation was removed.
- The simulation in three dimensions allowed determination of the effect of inlet length (IL) on the pressure drop in the annular flow. This effect is the distance that the fluid needs to reach a fully developed flow. From the results, it can be observed that an inlet length was more evident in the eccentric case, since it was more sensitive to the effect of fluid viscosity (lower levels of fluid consistency result in a higher IL) and fluid flow rate (higher levels of velocity in the annular section result in a higher IL). Knowledge of this effect is important for estimation of pilot/experimental unit size, related to the flow conditions investigated.
- In the concentric cases, it is worth emphasizing the effect of rotation on the reduction in pressure loss. The lower the fluid flow rate, the more evident this effect was; these facts agree with the information found in the literature. Authors like McCann et al. (1995), for example, have related this effect to the

concentric laminar flow and the inverse effect to the turbulent regime, which means that an increase in rotation increases the pressure drop. In the eccentric case simulations, there are some particularities; while the flow was not fully developed (IL < 5 times the external diameter) an increase in rotation decreased the pressure drop. However, when the flow was fully developed, the opposite occurred, and the pressure drop increased with shaft rotation. The increase in fluid flow rate made this effect more evident, as Figure 9 show.

- In most of the cases the eccentric configuration had a more evident reduction in pressure drop than the concentric ones. Only in the eccentric situation with Fluid 1 and with high values of flow and rotation (0.609 m/s and 5.24 rad/s) the results of pressure drop showed the same order of magnitude as in the same situation in the concentric case.
- Fluid viscosity had an effect on pressure drop of the same magnitude as that of fluid flow rate. All results obtained show higher values of pressure drop for the fluid with a higher viscosity.

CONCLUSIONS

Considering the information obtained in the operational range studied, the following conclusions were reached:

- The information obtained on the behavior of pressure drop had a qualitative aspect for interpretation of the effects of the main operational variables, showing physical agreement with the information reported in the literature.
- The use of computational fluid dynamics provided a satisfactory generation of information on contours and velocity profiles. Validation of the numerical method with experimental data from the literature on dimensionless velocity profiles supported the use of the algorithms employed, specially those associated with velocity and pressure coupling.
- The results allow the expansion of research horizons for computational fluid dynamics to investigation of the effects of turbulence and the prediction of particle motion in the annular helical flow.

ACKNOWLEDGMENTS

The authors are grateful for the support received from FAPEMIG – "Fundação de Amparo à Pesquisa do Estado de Minas Gerais" - and also under the "Plano Nacional de Ciência e Tecnologia" from the – "Setor de Petróleo e Gás Natural," CTPETRO, through CNPq under project number 463052/01-3.

NOMENCLATURE

e	eccentricity	(-)
n	power-law index in the Cross model	(-)
Re	Reynolds number	(-)
R_{ext}	inner radius of the outer tube	(m)
R_{int}	outer radius of the inner tube	(m)
U_a	dimensionless axial velocity	(-)
V_a	dimensionless tangential velocity	(-)
w	angular velocity	(rad/s)

Greek Symbols

λ	natural time in the Cross model	(s)
μ_0	zero shear rate viscosity in the Cross model	(kg/m.s)
μ_{ef}	effective viscosity	(Pa.s)
ρ	fluid density	(kg/m^3)
$\dot{\gamma}$	shear rate	(1/s)
$\bar{\tau}$	shear stress	(Pa)

REFERENCES

Cross, M. M., Rheology of non-Newtonian fluids: A new flow equation for pseudoplastic systems. Journal of Colloid Science, vol. 20, pp. 417-437 (1965).

Escudier, M. P., Gouldson, I. W., Oliveira, P. J. and Pinho, F. T., Effects of inner cylinder rotation on laminar flow of a Newtonian fluid through an eccentricity annulus, International Journal of Heat and Fluid Flow, vol. 21, pp. 92-103 (2000).

Escudier, M. P., Oliveira, P. J., Pinho, F. T. and Simth, S., Fully developed laminar flow of non-Newtonian liquids though annuli: Comparison of numerical calculations with experiments, Experiments in Fluids, vol. 33, pp. 101-111 (2002).

Martins, A. L., Campos, W., Maravilha, C., Satink, H. and Baptista, J. M., Effect of non-Newtonian behaviour of fluids in the erosion of a cutting bed in horizontal oilwell drilling, Hydrotransport, vol. 14, pp. 333-346 (1999).

McCann, R. C., Quigley, M. S., Zamora, M. and Slater, K. S., Effects of high-speed pipe rotation on pressures in narrow annuli, SPE Drilling &

Completion, June, pp. 96-103 (1995).

Nouar, C., Desaubry, C. and Zenaidi, H., Numerical and experimental investigation of thermal convection for a thermodependent Herschel-Bulkley fluid in an annular duct with rotating inner cylinder, Eur. Journal Mech B, vol. 17, pp. 875-900 (1998).

Nouri, J. M., Umur, H. and Whitelaw, J. H., Flow of Newtonian and non-Newtonian fluids in eccentric annulus with rotation of the inner cylinder, International Journal of Heat and Fluid Flow, vol. 18, pp. 236-246 (1997).

Sharif, M. A. R. and Hussain, Q. E., Numerical modeling of helical flow of viscoplastic fluids in eccentric annuli, AIChE Journal, vol. 46, no. 10, pp. 1937-1946 (2000).

Sharma, V. P. and Mahto, V., Rheological study of a water based oil well drilling fluid, Journal of Petroleum Science and Engineering, vol. 15, pp. 123-128 (2004).